
A diffusion-induced transition in the phase separation of binary fluid mixtures subjected to a temperature ramp

IZABELLA J. BENCZIK and JÜRGEN VOLLMER

Max Planck Institute for Dynamics and Selforganization, Göttingen, Germany

PACS 64.70.Ja – Specific phase transitions: Liquid-liquid transitions

PACS 05.45.-a – Nonlinear dynamics and chaos

PACS 47.70.Fw – Chemically reactive flows

Abstract. - Demixing of binary fluids subjected to slow temperature ramps shows repeated waves of nucleation which arise as a consequence of the competition between generation of supersaturation by the temperature ramp and relaxation of supersaturation by diffusive transport and flow. Here, we use an advection-reaction-diffusion model to study the oscillations in the weak- and strong-diffusion regime. There is a sharp transition between the two regimes, which can only be understood based on the probability distribution function of the composition rather than in terms of the average composition. We argue that this transition might be responsible for some yet unclear features of experiments, like the appearance of secondary oscillations and bimodal droplet size distributions.

Introduction. – Liquid-liquid phase separation occurs whenever an isotropic binary mixture is transferred into a bi-phasic region where its isotropic state is no longer stable, and the mixture decomposes into two equilibrium phases. In classical approaches [1] demixing was induced by sudden temperature quenches, after which the phase separation was monitored in constant temperature conditions. In many industrial [2] and natural [3,4] applications however, temperature is not constant but it *coevolves* with the phase separation. Accordingly, some recent works focused on systems subjected to time-dependent variations of the temperature, like repeated cycles of cooling and heating [5], or slow continuous temperature ramps [6–13].

Experiments [6–8] in fluid mixtures subjected to slow temperature ramps show unexpected phenomena: rather than continuously following the gradual change in temperature, the phase separation exhibits consecutive bursts of droplet nucleation alternating with quiescent periods [6–13].

This intriguing phenomenon can be explained in terms of the competition between the temperature ramp and diffusion. Due to the temperature ramp there are droplets present in the system at any time. Any change of temperature results in a change of the equilibrium composition of the background fluid and of the droplets: *supersaturation* – defined as the deviation from the actual to the equilibrium composition—builds up in the sample. This

supersaturation is relaxed by diffusive exchange of mass between the droplets and their environment, or occasionally also by nucleation of new droplets.

Immediately after a wave of nucleation, the droplet concentration is high [8]. In this case, diffusion, which acts on length scales of typical droplet distances, relaxes supersaturation by orders of magnitude faster than it is generated by the temperature ramp [12]. The concentration remains close to equilibrium, and no new droplets are nucleated. The system enters a quiescent period. In the course of time, the number of droplets in the system decays due to coarsening of the droplet distribution and sedimentation. Droplet distances grow. Thus the diffusive exchange becomes slow, and supersaturation rises again. Eventually, a new wave of nucleation is triggered. Clearly the strength of diffusive transport has a critical impact on the alternation of the active and quiescent periods of phase separation.

The strength of the diffusive transport is characterized by the ratio D/L^2 . Hence, it is affected not only by the distance between droplets L , but also by the diffusion coefficient D . The latter effect is especially important because the temperature ramp, that drives the phase separation, causes considerable variations of D . It rises monotonously as function of the distance from the critical point (cf. [14]).

Here, our aim is to investigate systematically the behaviour of the oscillations in different (weak and strong)

diffusion regimes. We adopt a numerical approach built on previous mean-field discussions [9,11] as far as the evolution of the supersaturation is concerned, and combined with a reactive-flow description [13]. The latter deals explicitly with the spatial distribution of droplets and supersaturation, and with the dynamics of droplets (formation, coagulation and advection). Upon increasing the diffusion coefficient we find a clearly defined transition in the characteristics of the oscillations — in particular in their period. We will compare this behaviour to experimental results, and point out that some yet unclear features of the experiments might be attributed to the continuous growth of the diffusion coefficient as the system departs from the critical point.

The model. — It is convenient to describe the dynamics in terms of a normalized composition σ [11–13], defined in such a way that it takes the value $\sigma_0 = 1$ in equilibrium, and values $0 < \sigma < 1$ when the system departs from equilibrium. In experiments, the normalized composition decreases like $\dot{\sigma} = -\xi\sigma$, where the decay rate ξ is a function of temperature [7,10]. It can be kept almost constant, however, by choosing a temperature protocol that assures that the equilibrium flux onto the droplets is constant in time [7,11].

In order to focus on the spatial fluctuations of the normalized composition we formulate the demixing dynamics in terms of the scalar field $\sigma(x, t)$. It is subjected to *advection* by the background flow, to an exponentially decaying *reaction* due to the temperature ramp, and to *diffusion* (for details see [13]):

$$\frac{\partial \sigma(x, t)}{\partial t} + \mathbf{u} \cdot \nabla \sigma(x, t) = \Gamma(\sigma) - \xi \sigma(x, t) + \mathcal{D} \Delta \sigma(x, t). \quad (1)$$

Here \mathcal{D} is the diffusion coefficient, and \mathbf{u} the velocity field of the background convection. The term $\Gamma(\sigma)$ represents formally the nucleation of droplets (see Eq. (4) for the actual implementation as a stochastic process). Nucleation brings the system back to equilibrium by resetting the local composition to $\sigma_0 = 1$. Thus it brings about a non-trivial (i.e. non-zero) final distribution of the $\sigma(x, t)$ field.

For numerical investigations of the advection-reaction-diffusion equation, Eq. (1), we use a lattice model proposed and described in an earlier work [13]. Here we just outline the basic elements of the model.

Spatial degrees of freedom are coarse grained in the form of cells of size ε which are labelled by the index (i, j) on an $N \times N$ lattice defined in a square of size L with periodic boundary conditions. At each time τ , we apply a reaction step in each lattice cell (i, j) ,

$$\sigma(i, j) \rightarrow \sigma(i, j) - \xi \tau \sigma(i, j), \quad (2)$$

that describes the changes of the normalized composition due to the external cooling. This step is followed by a diffusion step according to the transformation (see [15]):

$$\sigma(i, j) \rightarrow \sigma(i, j) + D \tau \cdot D(i, j), \quad (3)$$

where $D(i, j) = -\sigma(i, j) + [\sigma(i+1, j) + \sigma(i-1, j) + \sigma(i, j+1) + \sigma(i, j-1)]/4$ is the discrete Laplace operator, and D the diffusion coefficient in the discrete map. In the time continuous limit ($\tau \rightarrow 0$), this D corresponds to a diffusion coefficient $\mathcal{D} = D\varepsilon^2/4$.

In the next step, we nucleate droplets in cells that are far from equilibrium, (i.e. $\sigma < \sigma_{th} \equiv 2/3$) with a piecewise-linear probability $a(\sigma)$ of nucleation (as in [13]):

$$a(\sigma) = \begin{cases} 0, & \text{if } \sigma \geq \sigma_{th} = 2/3 \\ 2 - 3\sigma, & \text{if } 1/3 \leq \sigma < 2/3 \\ 1, & \text{if } \sigma \leq \sigma_{sp} = 1/3. \end{cases} \quad (4)$$

This choice reflects on one hand that for $\sigma \leq \sigma_{sp}$ spinodal decomposition causes instantaneous phase separation [1, 12], and on other hand that above a threshold value σ_{th} , the mixture is so close to equilibrium that practically no nucleation events occur. Upon nucleation the composition is set back to $\sigma_0(x, y) = 1$ in each cell where nucleation took place, as well as in the eight neighbouring cells.

The effects of the background convection are represented by an advection step that mixes the lattice cells and droplets in the lattice. This is generated by an incompressible alternating shear flow (as in [16]) that produces chaotic trajectories. The time-periodic velocity field of the flow is given by

$$\begin{aligned} u_x(x, y, t) &= \frac{A}{T} \Theta\left(\frac{T}{2} - t \bmod T\right) \sin \frac{2\pi y}{L}, \\ u_y(x, y, t) &= \frac{A}{T} \Theta\left(t \bmod T - \frac{T}{2}\right) \sin \frac{2\pi x}{L}, \end{aligned} \quad (5)$$

where $\Theta(x)$ is the Heaviside step function, T the period of the flow, and A the strength of the flow.

Finally, we take into account the merging of droplets: whenever two droplets approach each other to within a distance r_0 , the two droplets are replaced by a new droplet placed in the centre of mass of the two droplets.

Henceforth, we fix the cell size to the specific value ε^* that represents the maximal spatial scale where the σ -field takes constant values in the presence of diffusion and flow. Below the scale ε^* the small-scale fluctuations in σ , that are created continuously by the straining action of the velocity field, are dissipated by diffusion [17]. For a flow with Lyapunov exponent λ the scale ε^* can be estimated as follows [17]. The stretching and folding caused by the chaotic flow generates inhomogeneities of the σ -field on scales that decrease according to $\dot{\varepsilon} = -\lambda\varepsilon$. On the other hand, diffusion causes a broadening of the homogeneous areas according to $\dot{\varepsilon} = D/\varepsilon$ (adopting the solution $\varepsilon \sim t^{1/2}$). Thus the size of homogeneous areas evolves as: $\dot{\varepsilon} = D/\varepsilon - \lambda\varepsilon$. This equation possesses a steady state solution $\varepsilon^* = (D/\lambda)^{1/2} = LPe^{-1/2}$, where $Pe = \lambda L^2/D$ is the Péclet number, a measure of the strength of the diffusivity. Thus, the dimensionless cell size amounts to $\varepsilon^* = LPe^{-1/2}$. In what follows, we set the length and time scales to $L = 1$ and $T = 1$.

Oscillations in the weak- and strong-diffusion regimes. — To explore how the increasing diffusion co-

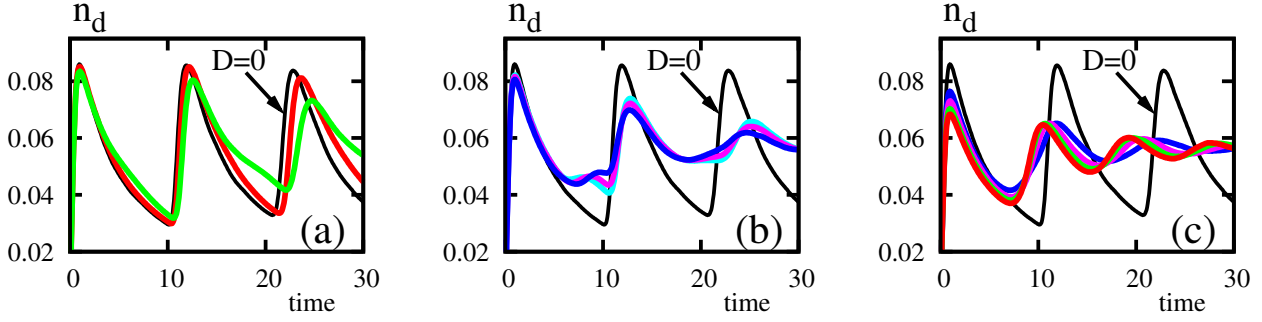


Fig. 1: Evolution of the droplet density n_d in numerical simulations for flow amplitude $A = 0.8$ and cooling rate $\xi = 0.04$ in the (a) weak ($D = 0.05$ - red, $D = 0.1$ - green line), (b) intermediate ($D = 0.14, 0.15$ and 0.16 in decreasing order of the amplitudes), and (c) strong ($D = 0.25, 0.35, 0.45$, and 0.55 in decreasing order of the periods) diffusion regimes. All simulations were started with a uniform initial composition field $\sigma_0 = 0.667$. The black thin line represents the diffusionless case. For intermediate values of D , as shown in panel (b), secondary oscillations appear.

efficient modifies the oscillations of the droplet density we fix the flow rate, the decay rate of the composition and the droplet interaction radius to $A = 0.8$, $\xi = 0.04$, and $r_0 = \varepsilon^*$, respectively, and study the oscillations for different diffusion coefficients ranging from $D = 0.05$ to $D = 0.55$. We follow 100 individual realizations of the system and average the results.

The oscillations are qualitatively different for low, intermediate and high values of the diffusion coefficient. In the weak-diffusion regime, Fig. 1(a), the period of the oscillations increases with increasing D , while their amplitude decreases faster than in the diffusionless case. As the diffusion coefficient increases further, this tendency stops at a certain value of D . For intermediate values of D [Fig. 1(b)] secondary oscillations appear. Subsequently, the period of the oscillations becomes smaller again [Fig. 1(c)], and the decay rate of the amplitude decreases with increasing D .

Transition between the weak- and strong-diffusion regimes. – The period of the oscillations takes its maximum value approximately in the middle of the range where secondary oscillations are observed [Fig. 2(a)]. Furthermore, the appearance of secondary oscillations in the intermediate diffusion regime is accompanied also by dramatic quantitative changes of the decay rate of the oscillation amplitude and of the decay of the composition in the quiescent period of the oscillations.

We quantify the decay of the oscillation amplitude by following how the difference between the maximum droplet density and its average value $\Delta n_d \equiv n_{d,\max} - n_{d,\text{av}}$ evolves in time. Our data show that for each diffusion coefficient this amplitude exhibits an exponential decay with rate γ_{amplit} ,

$$\Delta n_d \sim \exp[-\gamma_{\text{amplit}}(D) \cdot t]. \quad (6)$$

As a function of the diffusion coefficient D [Fig. 2(b)], this decay rate has an extremum localized at the end of the diffusion range in which secondary oscillations are present. The fastest decay of the amplitude corresponds to that value of the diffusion coefficient at which secondary oscil-

lations disappear from the system. For higher diffusion coefficients, the exponent γ_{amplit} decreases slightly. Then it seems to saturate.

The most abrupt change can be observed in the behaviour of the average composition in the system. We observe that in the quiescent period of each oscillation the average composition still (cf. [13]) decreases exponentially as

$$\sigma_{\text{av}} \sim \exp[-\gamma_{\sigma}(D) \cdot t], \quad (7)$$

due to the change of temperature. In the absence of droplets this decay is determined by the local decay, $\sigma(x) \sim \exp(-\xi \cdot t)$, of the composition in individual cells, such that $\gamma_{\sigma} = \xi$. When droplets are present in the system the diffusion of supersaturation into the droplets slows down the decay of the average composition. For small values of the diffusion coefficient the magnitude of this effect is small, and the average composition still decays with a rate $\gamma_{\sigma} \approx \xi$. However, when the diffusivity is increased to values where secondary oscillation appear, the decay rate of the average composition abruptly drops to a much lower value [Fig. 2(c)].

We conclude that the region where secondary oscillations are present represents a transition regime between the weak- and strong-diffusion regimes, where the transition point D_{tr} is defined by the maximal value of the oscillation period. To determine the dependence of the transition point on the different parameters of the system, we run numerical simulations for different decay rates ξ of the composition, and for different flow rates A . The position of the transition point is not affected significantly by the flow, but it is very sensitive to the decay rate ξ . More precisely, the transition occurs around $D_{\text{tr}} \approx 0.16$ for decay rate $\xi = 0.04$, at $D_{\text{tr}} \approx 0.08$ for $\xi = 0.02$, and around $D_{\text{tr}} \approx 0.04$ for $\xi = 0.01$. This is compatible with a linear scaling

$$D_{\text{tr}} \simeq 4\xi. \quad (8)$$

The diffusion coefficient D and the decay rate ξ define the length scale $\Lambda = \sqrt{D/\xi}$ at which the effects of the tem-

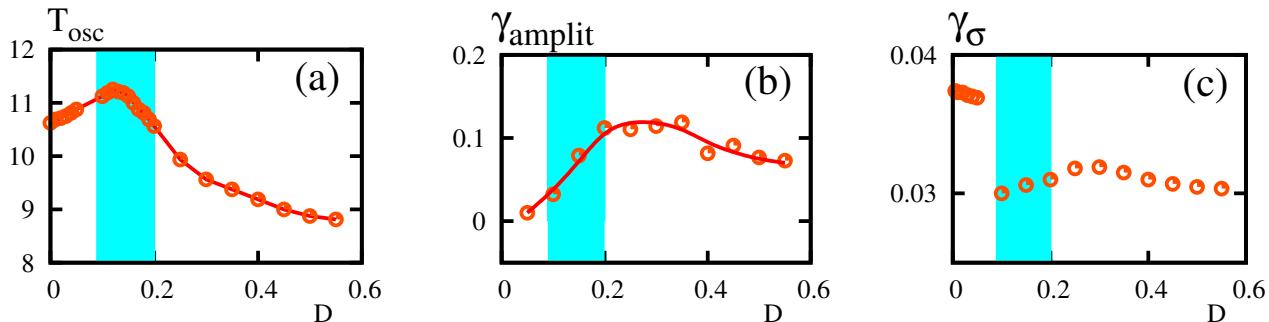


Fig. 2: Diffusion induced transition in the oscillatory behaviour of the phase separating mixture. For $\xi = 0.04$ and $A = 0.8$ the transition occurs in the highlighted region: $0.1 < D < 0.2$, determined as the region where secondary oscillations are observable. In the transition region: (a) the oscillations’ period reaches its maximal value, (b) the decay rate γ_{amplit} of the amplitude reaches its maximum, and (c) the decay rate γ_{σ} of the average composition σ_{av} decreases suddenly from $\gamma_{\sigma} \approx \xi = 0.04$ to $\gamma_{\sigma} \approx 0.03$.

perature ramp and the effects of diffusion are comparable. Diffusion can efficiently relax the supersaturation accumulated by the continuous temperature ramp up to a length scale of order Λ . In the continuum limit we find for the transition from the weak to the strong diffusion

$$\Lambda_{\text{tr}} = \sqrt{\frac{\mathcal{D}_{\text{tr}}}{\xi}} = \sqrt{\frac{D_{\text{tr}} \varepsilon^{*2}}{4 \xi}} = \sqrt{\frac{0.16}{4 \cdot 0.04}} \varepsilon^* = \varepsilon^*. \quad (9)$$

Hence, the transition occurs when the range in which diffusion can relax the accumulated supersaturation equals the length scale $\varepsilon^* = L/\text{Pe}^{1/2}$ where the effects of mixing by advection and diffusion are of the same order of magnitude.

Distributions of supersaturation. – At the onset of the nucleation wave the average composition σ_{av} varies in a broad range of values, and does not always approach the nucleation threshold $\sigma \neq \sigma_{th}$ [see Fig. 3 panels (1), (2) and (3)]. This indicates that the onset of the nucleation wave is not determined by the temporal evolution of the *average* composition. Rather, the nucleation wave is initiated by a small fraction of high-supersaturation “spots” that reach the threshold. Hence, an adequate description of the phenomenon should deal with the full distribution of the composition rather than only with the average composition. In this section, we present details about the behaviour of the composition distributions.

We focus on the evolution of the probability distribution functions (pdf-s) of the composition field in the low, intermediate- and strong-diffusion regimes. To obtain the pdf-s we consider composition bins of size $\delta\sigma = 1/200$. The resulting pdf-s are presented in Fig. 3 for different time instances: the upper panels (1) represent the weak-diffusion regime $D = 0.05$, while the middle (2) and bottom panels (3), the intermediate $D = 0.15$, and strong-diffusion $D = 0.55$ regimes, respectively.

The initial condition is a uniform composition field $\sigma(x, 0) = 0.667$, that is represented in the pdf-s as a δ -function (not shown). Due to the temperature ramp, this

peak moves to the left, in the direction of the nucleation threshold $\sigma_{th} = 2/3$, while it takes the form of a Gaussian distribution. When few points of the distribution cross the threshold level the nucleation wave starts. The points (cells) in which nucleation took place move up to $\sigma = 1$. In the panels (1a), (2a), and (3a) of Fig. 3 we show the distributions at the end of the first nucleation wave. Regardless of the diffusion regime the behaviour of the σ -field is similar in all the three cases: after several cells nucleate droplets the distribution becomes bimodal. There is a big number of cells being already around the equilibrium value $\sigma = 1$, and a small number of cells remain still slightly above the threshold and form a second peak.

This small peak is subjected to two opposing forces. Diffusion, represented by the red arrows (ii) in Fig. 3, tends to move the peak to the right: i.e., into the direction of the average composition that is already close to equilibrium. The second force is that of the temperature ramp. It is represented by the black arrows (i) in Fig. 3, and favours nucleation, i.e., it drives the peak further to the left in the direction of the nucleation threshold. The competition between the effects of diffusion and temperature ramp determines the fate of the small peak. Accordingly, the character of the oscillations differs in the three diffusion regimes.

In the weak-diffusion regime the effects of diffusion are small [(ii)<(i) in Fig. 3 panel (1a)]. Thus the temperature ramp will dominate, and the peak will slowly cross the threshold line σ_{th} and nucleate droplets. This delayed nucleation results in a long tail of the main peak, modifying its Gaussian shape [see Fig 3 panel (1b)]. The following oscillations [Fig. 3 panels (1c) and (1d)] will take place according to the same scenario. The slowing down is more and more efficient as the diffusion coefficient increases. Thus, the duration of the nucleation wave increases, explaining the increase of the oscillation period in the weak diffusion regime.

In the intermediate diffusion range the effects of the temperature drift and of diffusion balance each other

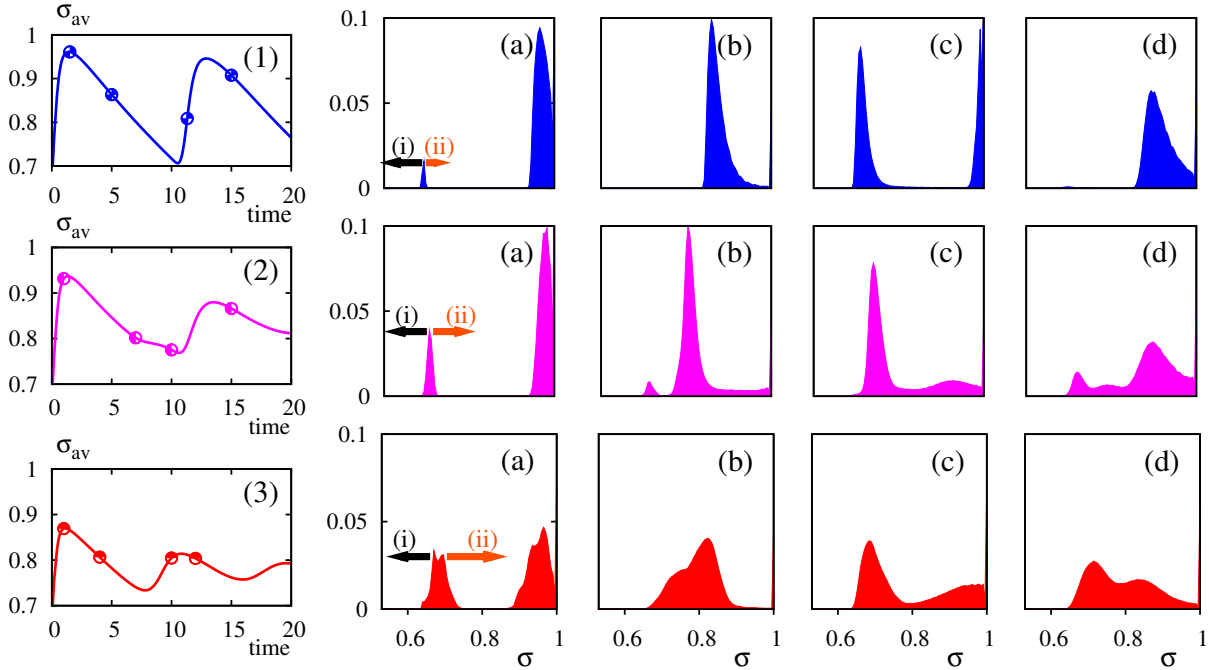


Fig. 3: Evolution of the average composition σ_{av} (left panels), and probability distribution functions of the composition at time instances marked by points in the left panels in the weak- ($D = 0.05$ – upper panels), intermediate- ($D = 0.15$ – middle panels), and strong-diffusion regimes ($D = 0.55$ – bottom panels). The flow rate is $A = 0.8$, the decay rate $\xi = 0.04$. The simulations were started with a uniform initial composition field $\sigma_0 = 0.667$. The plots of the pdf-s all show the range $0.5 \leq \sigma \leq 1$, the arrows (i) and (ii) are described in the text.

[(ii) \approx (i) in Fig. 3 panel (2a)]. The small peak is arrested from nucleation and stopped in the close vicinity of the nucleation threshold without actually reaching it. Meanwhile, the continuous ramp of temperature moves the big peak to lower composition levels where the effect of diffusion becomes less efficient. Eventually, the small peak manages to cross the nucleation level. This happens *after* the first nucleation wave was finished and gives rise to a separate small wave of nucleation. In this way, a secondary oscillation of the droplet density [as shown in Fig. 1(b)] occurs in the system. After this secondary nucleation wave a distinct small peak forms close to $\sigma = 1$ which does not attach to the big peak. Both peaks maintain their Gaussian character while travelling downward [Fig. 3 panel (2b)], maintaining the bimodal distribution of the composition. In the next wave of nucleation, the bigger peak breaks again in two distinct modes, forming a trimodal distribution. The number of modes increases by one at each subsequent principal or secondary nucleation wave. Thus, the distribution converges rapidly to a flat distributions in which the standard deviations of the individual modes are larger than the distances between them, and the phase separation proceeds continuously rather than in distinguishable oscillations. This explains the rapid decay of the amplitude in this transition regime.

In the strong-diffusion regime the effects of diffusion overcome the effects of the temperature ramp [(ii) $>$ (i) in Fig. 3 panel (3a)]. The small peak is not only arrested from

nucleation, but it moves backwards towards the big peak. The big peak in turn, travels downward in the direction of the nucleation threshold because of the intense diffusive exchange. Soon the two peaks merge [Fig. 3 panel (3b)] and form again one single peak with an (almost) Gaussian shape [Fig. 3 panel (3c)]. In the next nucleation waves everything is repeated in a similar way [Fig. 3 panels (3c) and (3d)]. In this regime, there is always a certain number of cells in which the supersaturation is released by diffusive transport. For high values of the diffusion coefficient, the downward travel of the big peak is accelerated by the rapid diffusive exchange with the small droplets. It hence moves much faster than in the weak diffusion regime where this motion was caused by the temperature ramp alone. As a result the period of the oscillations decreases in this regime.

When starting the simulations with a random initial condition instead of uniform a σ -field this picture does not change because diffusion tends to synchronize the composition. In the strong diffusion regime the synchronization of lattice cells is so fast that the character (period, amplitude) of the oscillations is hardly affected by the initial condition. Even in the weak diffusion regime the oscillations are still clearly observable. Their period remains almost the same, while their amplitude is considerably reduced as compared to the case of the uniform initial condition.

Discussion and conclusions. – Oscillatory phase separation of binary mixtures subjected to slow temperature ramps is a relatively new topic in liquid-liquid phase separation. Even though precision experiments unveiled many characteristics of the phenomena [6–8], and there are numerous theoretical attempts to explain their dynamics [9–13], the parameter dependence of the oscillations period is still an open question. Secondary effects appear even in well-controlled experiments [8, Fig. 15], and shield the principal behaviour of the system. For instance, **(a)** secondary oscillations can appear [18], **(b)** the frequency of the oscillations increases during one experimental run (Fig. 10 in [7]; Fig. 3 in [11]; Fig. 15 in [8]), and **(c)** bimodal droplet size distributions occur [3, Fig. 3].

In this communication we identified these secondary effects in a model system, and we pointed out that they can be attributed to the growing diffusion coefficient as the system departs from the critical point. Upon increasing the diffusion coefficient we observe a cross-over regime where the behaviour of the demixing changes qualitatively.

(a) In the cross-over regime the system performs a secondary oscillation between any two major bursts of nucleation [Fig. 1(b)]. Similar secondary oscillations are clearly visible in experiments when the system is still close to the critical point, and accordingly the diffusion coefficient is relatively small [18]. The secondary oscillations are observable over several periods. In the experiments they disappear eventually, as the diffusion coefficient increases due to the change of temperature.

(b) Our result, Fig. 2(a), shows that in experimental runs where the diffusion coefficient increases gradually as the system departs from the critical point, one should expect that the period of the oscillations might initially increase slightly and eventually decrease considerably. This has indeed been observed in experiments (cf. Fig. 10 in [7]; Fig. 3 in [11]; Fig. 15 in [8]).

(c) Exploring the distribution of the supersaturation has revealed that the oscillatory phase separation can not be described adequately in terms of the average composition. The spatial distributions of the composition plays a crucial role, and should explicitly be taken into account. This is particularly important in the cross-over regime where the secondary oscillations are observed. They are consequences of the bimodal distributions that temporarily appear in the evolution of the composition field. Accordingly, droplets are formed at two different time instances during an oscillation. Since droplets start to grow immediately after they are nucleated, this difference in the nucleation time will lead to bimodal droplet size distributions as they have been observed in [3, Fig. 3]. We expect that such bimodal droplet size distributions appear only in the intermediate and strong-diffusion regimes. An experimental test of these predictions is under way [18].

In summary, we conclude that identifying secondary effects which arise from the interplay of diffusion and the non-trivial spatial distribution of supersaturation provides an important step to a comprehensive understanding of

the dynamics of phase separation in the presence of a temperature ramp.

We are grateful to Tobias Lapp, Martin Rohloff, Ray Pierrehumbert, and Tamás Tél for discussions, inspiration and feedback.

REFERENCES

- [1] D.W. OXTOBY, *J. Phys.: Condens. Matter*, **4** (1992) 7627; *ibid.*, **10** (1998) 897; A. BRAY, *Adv. Phys.*, **43** (1994) 357; H. TANAKA and T. SIGHUZI, *Phys. Rev. Lett.*, **75** (1995) 874; A. ONUKI, *Phase Transition Dynamics* (Cambridge) 2002; V.I. KALIKMANOV, *J. Chem. Phys.*, **124** (2006) 124505.
- [2] KARMA A. and SARKISSIAN A., *Phys. Rev. Lett.*, **68** (1992) 2616; MERCHANT G. *et al.*, *SIAM J. Appl. Math.*, **52** (1992) 1279; SANTANICOLA G., MAURI R. and SHINNAR R., *Ind. Eng. Chem. Res.*, **40** (2001) 2004; RULLMANN M. and ALIG I., *J. Chem. Phys.*, **120** (2004) 7801.
- [3] SHAW R.A., *Annu. Rev. Fluid. Mech.*, **35** (2003) 183.
- [4] SPARKS R.S. *et al.*, *Nature*, **361** (1993) 246; MELNIK O. and SPARK R., *Nature*, **402** (1999) 37.
- [5] JOSHUA M. and GOLDBURG W., *Phys. Rev. A*, **31** (1985) 3857; SINGH A. *et al.*, *J. Chem. Phys.*, **134** (2011) 044910.
- [6] VOLLMER D., STREY R. and VOLLMER J., *J. Chem. Phys.*, **107** (1997) 3619; VOLLMER D., VOLLMER J. and WAGNER W., *J. Chem. Phys.*, **4** (2002) 1380.
- [7] AUERNHAMMER G.K., VOLLMER D. and VOLLMER J., *J. Chem. Phys.*, **123** (2005) 134511.
- [8] LAPP T., ROHLOFF M., VOLLMER J. and HOF B., [arXiv1107.1194](https://arxiv.org/abs/1107.1194).
- [9] VOLLMER J., VOLLMER D. and STREY R., *J. Chem. Phys.*, **107** (1997) 3627; VOLLMER J. and VOLLMER D., *Faraday Discuss.*, **112** (1999) 51.
- [10] CATES M.E. *et al.*, *Philos. Trans. R. Soc. (London)*, **361** (2003) 793.
- [11] VOLLMER J., AUERNHAMMER G.K. and VOLLMER D., *Phys. Rev. Lett.*, **98** (2007) 115701.
- [12] VOLLMER J., *J. Chem. Phys.*, **129** (2008) 164502.
- [13] BENCZIK I.J. and VOLLMER J., *Europhys. Lett.*, **91** (2010) 36003.
- [14] B. STEINHOFF and D. WOERMANN, *J. Chem. Phys.*, **103** (1995) 8985.
- [15] PIERREHUMBERT R.T., *Chaos*, **10** (2000) 61.
- [16] PIERREHUMBERT R.T., *Chaos Sol. Fract.*, **4** (.) 19941091; NEUFELD Z., HAYNES P.H. and PICARD G., *Phys. Fluids*, **12** (2000) 2506.
- [17] TÉL T. *et al.*, *Chaos*, **10** (2000) 98.
- [18] TOBIAS LAPP,, private communication.